ACS OMEGA

http://pubs.acs.org/journal/acsodf

Article

ReS_2 Cocatalyst Improves the Hydrogen Production Performance of the CdS/ZnS Photocatalyst

Na Su, Yang Bai,* Zhonglian Shi, Jiale Li, Yixue Xu, Daoxiong Li, Baolu Li, Liqun Ye,* and Yi He

Cite This: *ACS Omega* 2023, 8, 6059−6066

Read Online

ACCESS | Metrics & More | Article Recommendations

ABSTRACT: Photocatalysis provides an exciting solution to the current growing energy challenge. However, the activity and stability of photocatalysts are two important issues in photocatalytic applications. In this work, we have successfully developed an efficient and stable photocatalyst by loading ReS_2 nanoparticles onto a CdS/ZnS heterojunction. After loading ReS_2, there is a strong interaction between the CdS/ZnS heterojunction and ReS_2, which accelerates the photogenerated charge migration and effectively inhibits the recombination of photogenerated electrons and holes. Accordingly, CdS/ZnS-ReS_2 displays excellent photocatalytic activity and stability with the highest hydrogen production rate of 10 722 μmol g^{-1} h^{-1}, which is approximately 178 times higher than that of the pure CdS and 5 times better than that of CdS/ZnS. This work not only facilitates solar energy conversion to improve photocatalytic activity and stability but also broadens the application of ReS_2 as a cocatalyst.

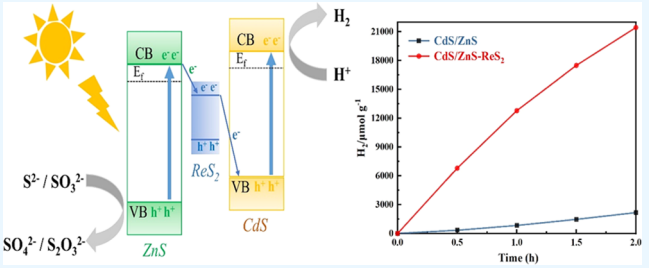

1. INTRODUCTION

Due to the continuous progress of society, environmental and energy problems are becoming increasingly serious. Due to the shortage of fossil energy, there is a need to develop other clean energy sources. Hydrogen is now widely considered to be a clean and green energy source. Although there are many methods to produce hydrogen, hydrogen generation by photocatalysis based on solar energy and water is considered to be one of the most promising methods to produce hydrogen.[1−4] Since the great discovery of Fujishima and Honda in 1972,[5] many photocatalysts have been studied and explored, such as metal oxides[6−8] and metal sulfides.[9−11] However, among many photocatalysts, CdS has been widely investigated due to its narrow band gap (∼2.4 eV), wide visible light absorption range, and suitable conduction band position for water reduction.[12] Unfortunately, CdS is prone to photocorrosion under light and photogenerated carriers are easily compounded, which limit its wide application and development.[13−15] To solve this problem, researchers modified CdS, for example, by constructing heterojunctions and loading cocatalysts.[16−20] Lin et al. greatly improved the efficiency and stability of photocatalytic hydrogen production by constructing CdS/ZnS heterojunctions.[21] Because ZnS has a wide band gap with good stability and photocorrosion resistance,[22,23] combining CdS and ZnS can improve the photocatalytic hydrogen production activity. This has been widely investigated by many scholars.[21,22,24−28] Although the CdS/ZnS heterojunction exhibits better photocatalytic performance than pure CdS and ZnS, it still suffers from low photoconversion efficiency and poor stability, which largely hinders its practical application. Therefore, it is necessary to find new solutions.

Recently, the enhancement of photocatalytic activity and stability by loading cocatalysts on photocatalysts has attracted the interest of many researchers, for example, noble metal cocatalysts (Ag, Pt, and Au), nickel-based cocatalysts (Ni, NiS, and NiO), and two-dimensional transition metal dihalides (MoS_2, WS_2, and ReS_2).[20,22,29−35] Among these catalysts, ReS_2 with a stable phase structure, excellent charge transfer ability, and a large number of unsaturated sites, is considered a promising cocatalyst.[36−39] For example, some researchers had successfully loaded ReS_2 onto CdS nanorods as a cocatalyst, and when they used NaS_2−$NaSO_3$ as a sacrificial reagent, the hydrogen production rate of ReS_2/CdS was about 127 times higher than that of pure CdS.[40] Therefore, we would like to load ReS_2 onto the CdS/ZnS catalyst to further improve its photocatalytic performance. However, there are few studies on the use of ReS_2 as a cocatalyst for photocatalytic hydrogen production. In particular, the role of ReS_2 in CdS/ZnS heterojunctions remains unstudied.

In this work, we have successfully loaded ReS_2 onto a CdS/ZnS heterojunction by a simple hydrothermal method. The

Received: December 21, 2022
Accepted: January 17, 2023
Published: January 31, 2023

https://doi.org/10.1021/acsomega.2c08110
ACS Omega 2023, 8, 6059−6066

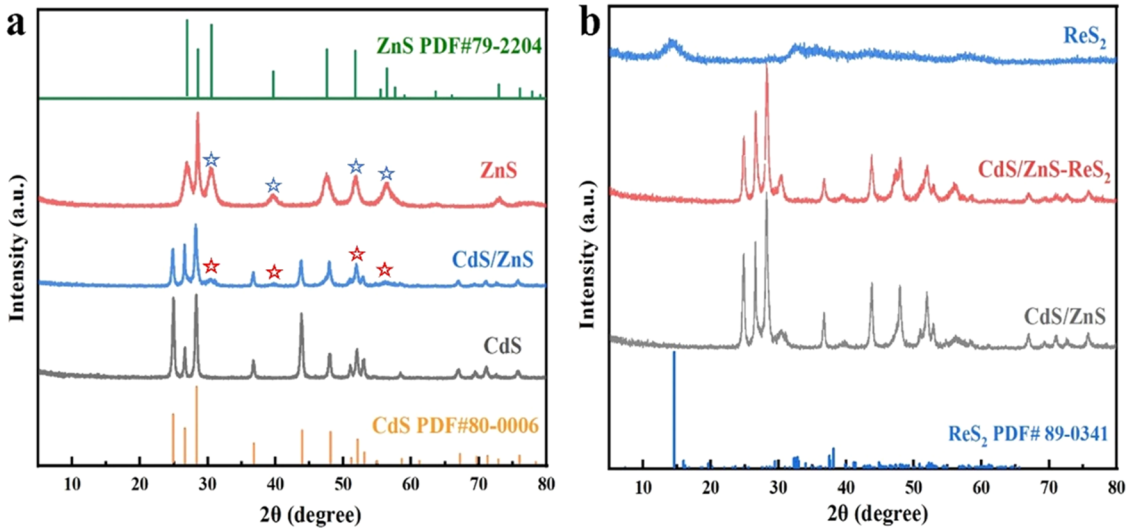

Figure 1. (a) XRD patterns of ZnS, CdS, and CdS/ZnS and standard diffraction patterns of ZnS and CdS. (b) XRD patterns of ReS_2 and CdS/ZnS-ReS_2 and standard diffraction patterns of ReS_2.

rod-like CdS provides the substrate and reaction site for the loading of ZnS and ReS_2. The addition of ReS_2 helps to achieve photogenerated charge transfer, inhibits carrier recombination, and improves the photocatalytic performance and stability of CdS/ZnS. Therefore, CdS/ZnS with ReS_2 as a cocatalyst has high photocatalytic performance and stability for hydrogen production. The highest performance was shown when NaS_2−$NaSO_3$ was used as the sacrificial reagent, and the rate of hydrogen produced was about 178 times that of pure CdS and 5 times that of CdS/ZnS, and there was no degradation in performance after four photocatalytic cycles.

2. EXPERIMENTAL SECTION

2.1. Synthesis of CdS NRs. The CdS nanorods were prepared by a simple solvothermal method.[41] In a typical procedure, 5 g of Cd $(NO_3)_2{\cdot}4H_2O$ and 3.69 g of NH_2CSNH_2 (Cd:S = 1:3) were dissolved in 80 mL of ethylenediamine. Then the solution was transferred to a 100 mL Teflon-lined stainless steel autoclave after 30 min of vigorous stirring and kept at 170 °C for 22 h. When the autoclave was naturally cooled to room temperature, the yellow powders were collected through centrifugation. After being washed with ultrapure water and anhydrous ethanol (3 times for each solvent), the precipitate was dried in a vacuum oven at 60 °C overnight for further use.

2.2. Synthesis of CdS/ZnS. In breif, 308 mg of CdS synthesized above, 768 mg of $Zn(Ac)_2{\cdot}2H_2O$, and 404 mg of NH_2CSNH_2 were dissolved in 70 mL of H_2O and 10 mL of $C_2H_8N_2$. After stirring vigorously for 30 min, the solution was transferred to a 100 mL Teflon-lined stainless steel autoclave and kept at 160 °C for 10 h. After cooling to room temperature, the precipitate was collected by centrifugation and washed with ultrapure water and anhydrous ethanol (3 times for each solution). Finally, it was dried in a vacuum oven at 60 °C overnight.

2.3. Synthesis of CdS/ZnS-ReS_2. Typically, 10 mg of NH_4ReO_4, 5.6 mg of C_2H_5NS, and 300 mg of CdS/ZnS synthesized above were dissolved in 35 mL of H_2O. After stirring for 30 min, the solution was transferred to a 50 mL Teflon-lined stainless steel autoclave and kept at 220 °C for 16 h. When the autoclave was naturally cooled to room temperature, CdS/ZnS-ReS_2 was rinsed several times with ultrapure water and anhydrous ethanol. Finally, the green precipitate was dried in a vacuum oven at 60 °C overnight.

2.4. Characterization. X-ray diffraction (XRD) patterns were collected on a Bruker D8 diffractometer using Cu Ka radiation with a scan range of 5−80° at a scan rate of 6 ° min^{-1}. The morphology of the samples was characterized using an FEI QUANTA 200 emission scanning electron microscope (FESEM). Transmission electron microscopy (TEM), high-resolution TEM (HRTEM) images, and elemental distributions were acquired through a JEOL JEM-2100 F (UHR) field emission transmission electron microscope. UV−vis diffuse reflectance spectra (DRS) data for the samples were obtained with a UV−vis spectrometer (PerkinElmer Lambda 650 s), using $BaSO_4$ as a reference. X-ray photoelectron spectroscopy (XPS) measurements were determined with a Thermo Scientific ESCALAB 250 XI X-ray photoelectron spectrometer (Al Ka, 150 W, C 1s 284.8 eV). PL spectra were measured by a spectrophotometer (F-4600 FL) at room temperature.

2.5. Photocatalytic H_2 Production. First, 50 mg of photocatalyst, 2.1 g of Na_2S, and 0.8 g of Na_2SO_3 were weighed into 50 mL of ultrapure water, followed by ultrasonic dispersion for 30 min. After complete dispersion, it was added to a glass reactor and purged with Ar for a certain period of time. A 300 W xenon lamp (PLS−SXE300C, Beijing Perfect Light Technology Co., Ltd., China) was used as the light source ($\lambda \geq 420$ nm). During illumination, a gas sample (1 mL) was taken out with a syringe from the reactor every 30 min and analyzed with a gas chromatograph (GC9790II, Zhejiang Fuli Analytical Instrument Co., Ltd., China) equipped with a thermal conductivity detector (TCD) and a 5 Å molecular sieve column, where Ar was used as the carrier gas. The amount of H_2 was quantitatively analyzed according to the standard curve.

2.6. Photoelectrochemical Measurements. The photocurrent response, electrochemical impedance spectroscopy, and Mott−Schottky curve of the catalysts were measured using a CHI 660D electrochemical workstation (CHI Instruments, Shanghai, China). We use a 0.5 M Na_2SO_4 solution as the electrolyte solution. First dissolve 0.01 g of ethyl cellulose and 0.1 g of catalyst were dissolved in approximately 15 mL of

https://doi.org/10.1021/acsomega.2c08110
ACS Omega 2023, 8, 6059−6066

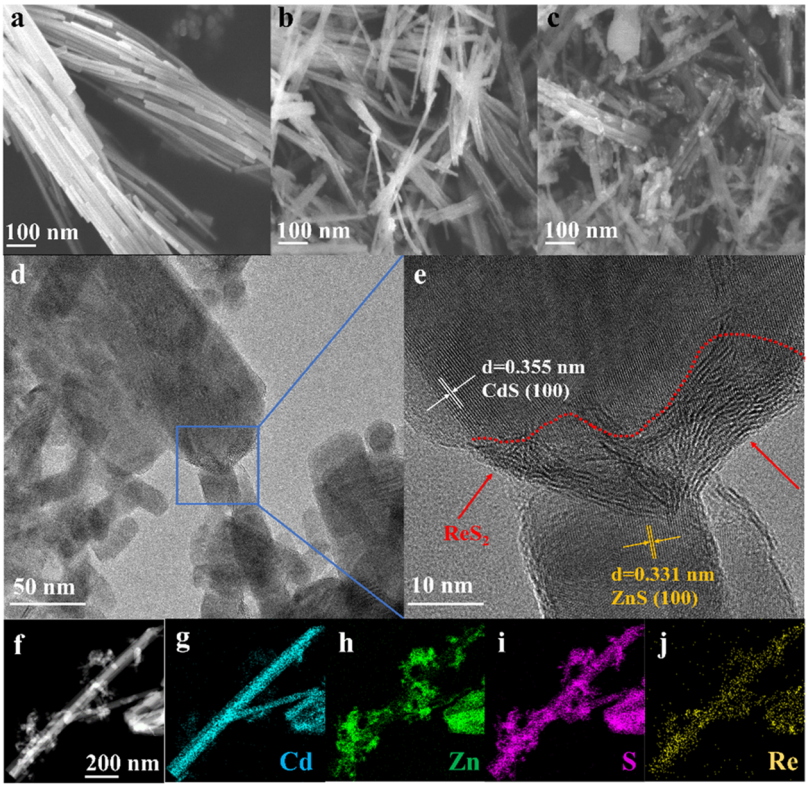

Figure 2. SEM images of (a) CdS, (b) CdS/ZnS, and (c) CdS/ZnS-ReS_2, (d) CdS/ZnS-ReS_2 TEM image, (e) CdS/ZnS-ReS_2 HRTEM image, and (f–j) EDS elemental mapping.

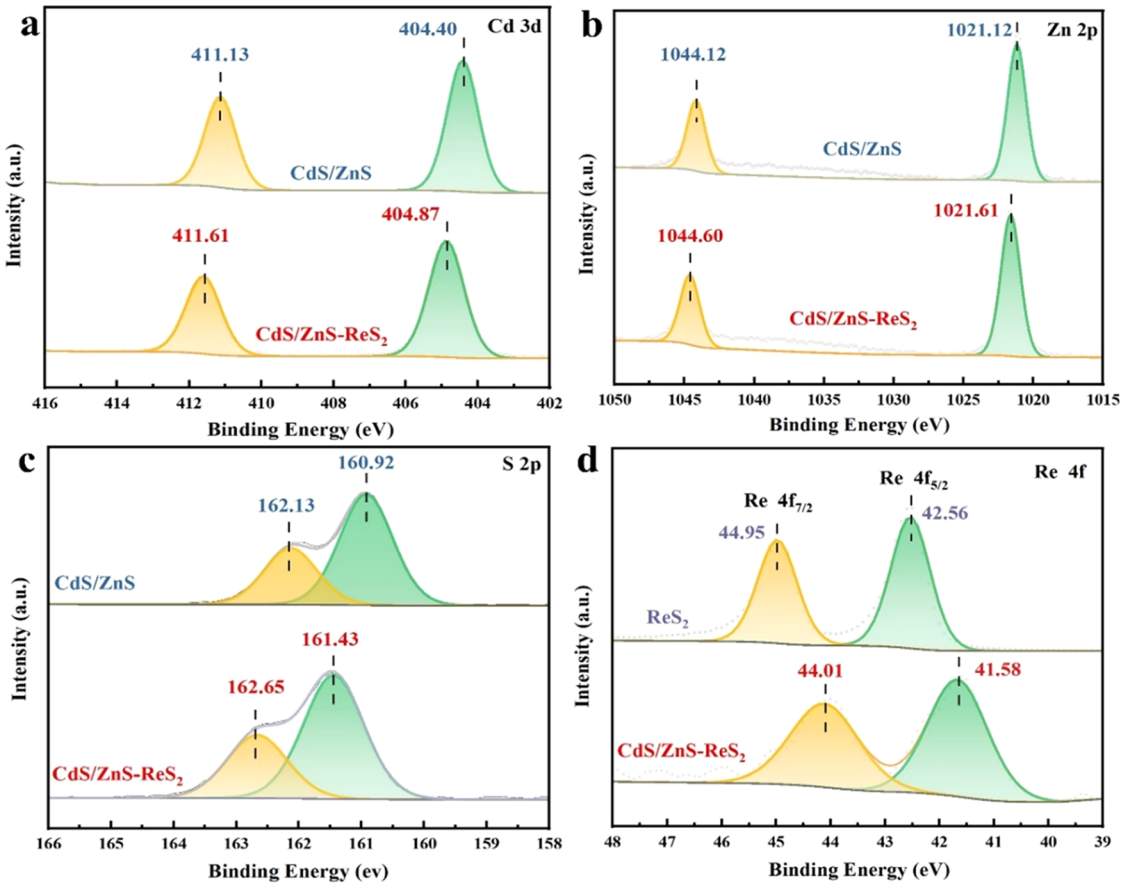

Figure 3. XPS analysis of CdS/ZnS, CdS/ZnS-ReS_2, and ReS_2: (a) Cd 3d, (b) Zn 2p, (c) S 2p, and (d) Re 4f.

https://doi.org/10.1021/acsomega.2c08110
ACS Omega 2023, 8, 6059−6066

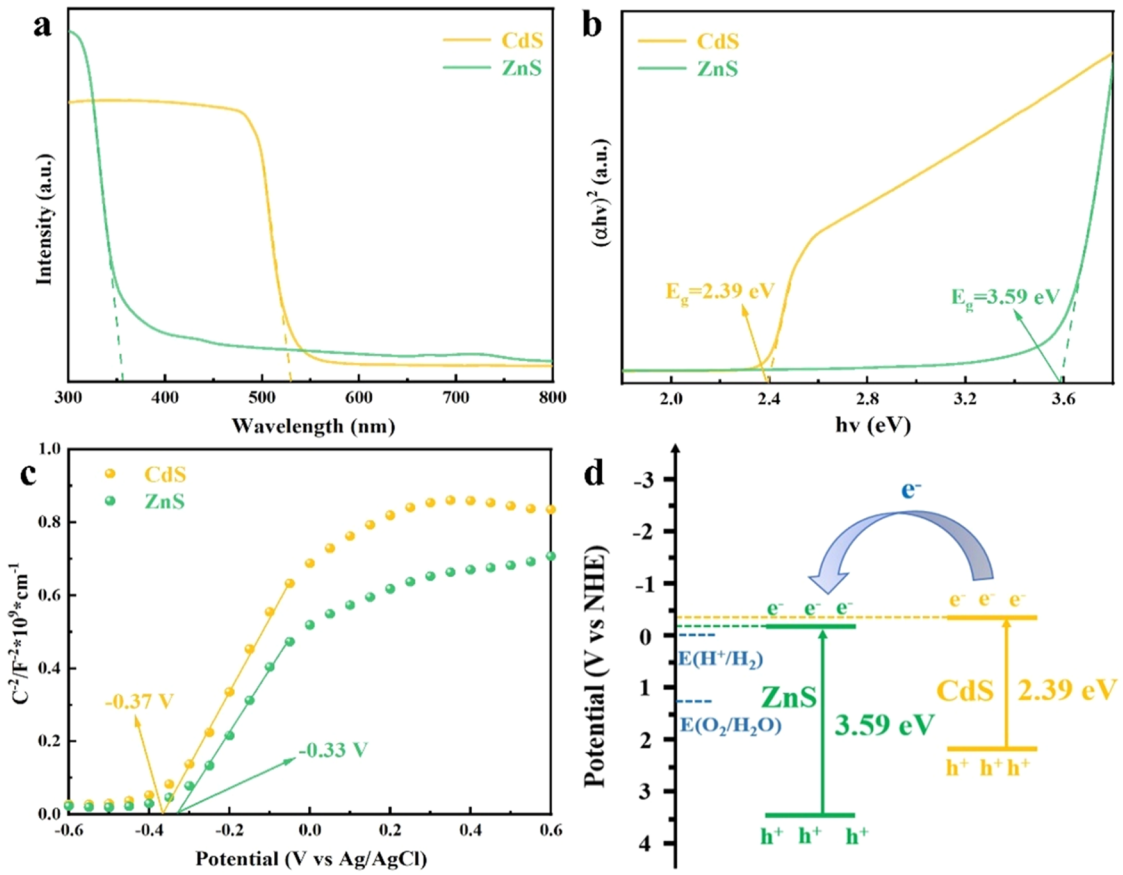

Figure 4. (a) UV−vis diffuse reflection spectra, (b) corresponding Tauc plots, (c) Mott−Schottky plots, and (d) band structure diagrams of CdS and ZnS.

ethanol and then coated on FTO glass by a coating rod and dried at 120 °C for 3 h. Sample-coated FTO glass, carbon rod, and Ag/AgCl electrodes were used as the working, counter, and reference electrodes, respectively. During the photocurrent test, a 300 W Xe lamp was used as the light source, and the test was performed under visible light.

3. RESULTS AND DISCUSSION

The crystal structures and compositions of the samples are shown in Figure 1, which shows the XRD spectra of CdS, ZnS, CdS/ZnS, and CdS/ZnS-ReS_2, and the standard diffraction patterns of CdS (PDF #80-0006), ZnS (PDF #79-2204), and ReS_2 (PDF #89-0304). CdS/ZnS was synthesized by a two-step hydrothermal method, and the synthesized CdS and ZnS were both in the hexagonal phase. From Figure 1a, we can see that the diffraction peaks of ZnS appear in CdS/ZnS in addition to the original diffraction peaks of CdS, and the diffraction peaks at 2θ values of 30.5, 39.5, 51.7, and 56.35° correspond to the (101), (102), (103), and (112) crystallographic planes of ZnS, respectively. Compared with the diffraction peaks of CdS and ZnS, the diffraction peaks of CdS/ZnS are not shifted to the high-or low-angle side, which indicates that the sample is not a solid solution but a heterogeneous junction. From Figure 1b, it can be seen that the diffraction peaks of CdS/ZnS do not change significantly after loading ReS_2 on the surface of CdS/ZnS, which indicates that the addition of ReS_2 does not change the crystal structure of CdS/ZnS. However, we did not observe the diffraction peaks of ReS_2 on the XRD patterns of CdS/ZnS-ReS_2, which may be due to its low content and crystallinity.

The morphologies and microstructures of the samples are shown in Figure 2. Figure 2a shows the SEM images of pure CdS, which behave as nanorods with a smooth surface. The SEM images of CdS/ZnS and CdS/ZnS-ReS_2 are shown in Figure 2b,c. It is obvious that the surface of CdS nanorods becomes rough after loading with ZnS and ReS_2, but the morphology of CdS nanorods is not changed, indicating that Zn and Re are successfully loaded. In addition, the lattice spacing of 0.355 nm in Figure 2e corresponds to the (100) crystal plane of CdS and 0.331 nm corresponds to the (100) crystal plane of ZnS, which are consistent with the XRD test results (Figure 1a). The EDS spectra demonstrate the presence of Cd, Zn, S, and Re elements, and Figure 2f−j shows the elemental distribution of CdS/ZnS-ReS_2, demonstrating that S and Cd elements are uniformly distributed in the selected region, while Zn and Re are separately distributed, which further indicates that the contact between CdS, ZnS, and ReS_2 are in close contact with each other. An effective interfacial contact can shorten the charge transfer distance, and ReS_2 facilitates the electron transfer between CdS and ZnS.

We have explored the surface and elemental valence states of CdS/ZnS and CdS/ZnS-ReS_2 samples by X-ray photoelectron spectroscopy (XPS). Figure 3 compares the binding energies of Cd, Zn, S, and Re elements in the two samples, corrected with the C 1s peak at 248.80 eV as a reference. The peaks at 411.13 and 404.40 eV in Figure 3a correspond to Cd $3d_{5/2}$ and Cd $3d_{3/2}$ in the CdS/ZnS sample, respectively; however, the Cd 3d

https://doi.org/10.1021/acsomega.2c08110
ACS Omega 2023, 8, 6059−6066

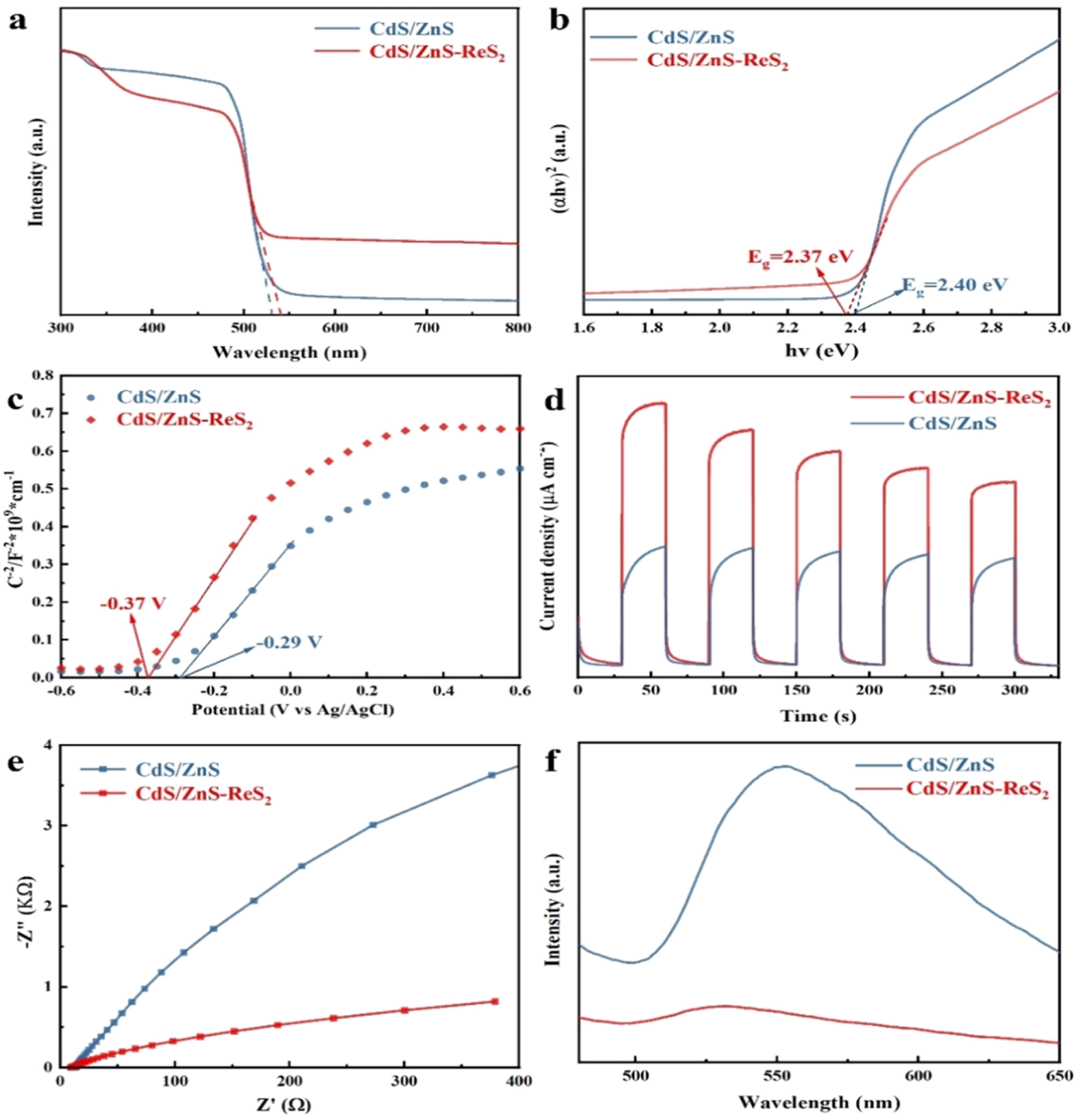

Figure 5. (a) UV−vis diffuse reflection spectra, (b) corresponding Tauc plots, (c) Mott−Schottky plots, (d) Transient photocurrent response curves, and (e) electrochemical impedance plots of CdS/ZnS and CdS/ZnS-ReS_2 samples. (f) PL spectra of CdS/ZnS and CdS/ZnS-ReS_2 samples excited at 550 nm.

shifts to a higher binding energy after loading with ReS_2. Similarly, Zn 2p and S 2p are also shifted toward higher binding energy as seen in Figure 3b,c. The two different peaks at 44.01 and 41.58 eV in Figure 3d correspond to Re $4f_{7/2}$ and Re $4f_{5/2}$ of the CdS/ZnS-ReS_2 sample, respectively, which shows that Re 4f in the sample moves in the direction of lower binding energy compared to pure ReS_2, which indicates that the electron cloud density on the ReS_2 surface increases after loading ReS_2 and electrons are transferred to the ReS_2 surface. The above evidence proves that there is a strong interaction between CdS/ZnS and ReS_2.

To investigate the interaction between CdS and ZnS, UV−vis diffuse reflectance tests and Mott−Schottky tests were performed on separate CdS and ZnS samples. The absorbance range of CdS is much larger than that of ZnS, as can be seen in Figure 4a. The band gaps of the samples were calculated from the Tauc curves based on the formula $\alpha h\nu = A(h\nu - E_g)^{n/2}$ to obtain the band gaps of 2.39 and 3.59 eV for CdS and ZnS, respectively, as shown in Figure 4b. The Mott−Schottky curves are used to determine the semiconductor type and the flat-band potential. The slopes in Figure 4c are both positive, indicating that both ZnS and CdS are n-type semiconductors. The flat-band potentials of the semiconductors were determined by making the intercept of the tangents on the x-axis, which are −0.37 and −0.33 V, respectively, and then the conduction band potentials of CdS and ZnS were obtained using E_q. The energy band structure of CdS and ZnS is shown in Figure 4d. The valence band potential of the sample is calculated using the equation $E_g = E_{VB} + E_{CB}$.

Similarly, we also investigated the effect of loading ReS_2 on the optical properties of CdS/ZnS samples using UV−visible diffuse reflectance. As shown in Figure 5a, the light absorption range of CdS/ZnS increases after loading with ReS_2, which may be due to the good visible light trapping ability of ReS_2 black nanoparticles. As before, the relation between $(\alpha h\nu)^2$ and energy $(h\nu)$ can be calculated for the band gap values of 2.40 and 2.37 eV for CdS/ZnS and CdS/ZnS-ReS_2, respectively (Figure 5b). The narrower the band gap, the more favorable

https://doi.org/10.1021/acsomega.2c08110
ACS Omega 2023, 8, 6059−6066

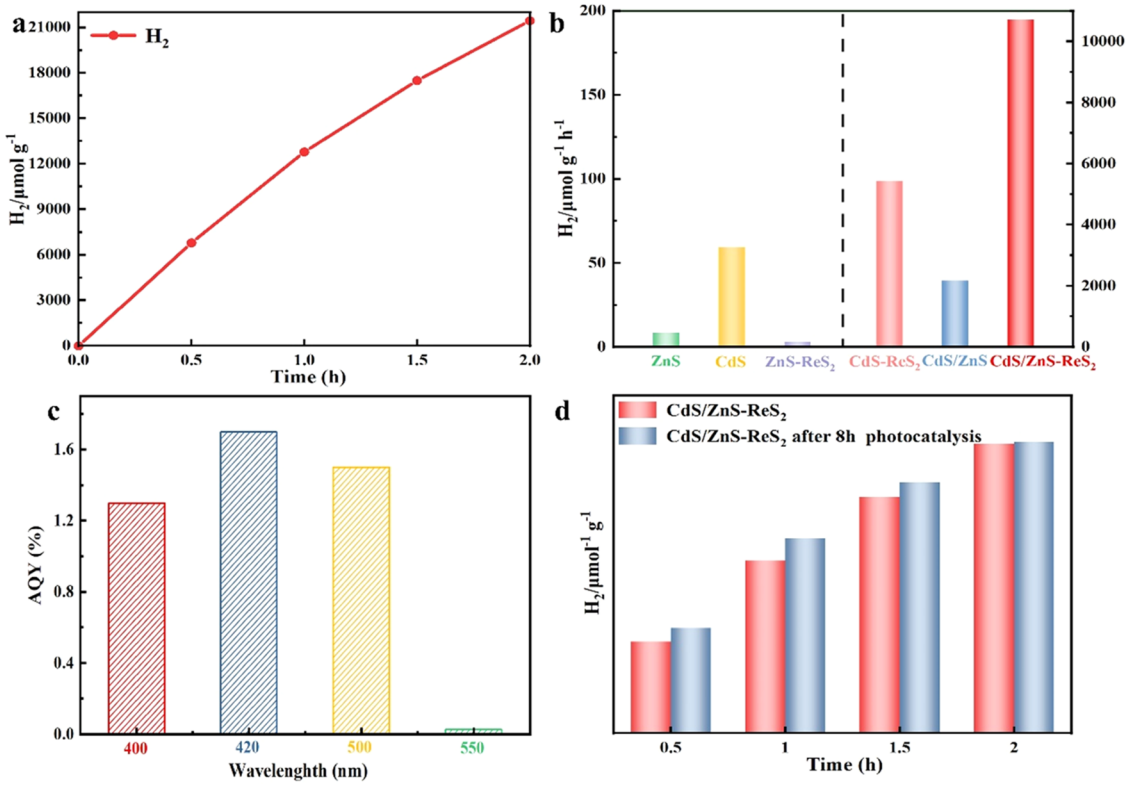

Figure 6. (a) Amount of hydrogen produced by photocatalysis of CdS/ZnS-ReS_2, (b) photocatalytic H_2 evolution rate of ZnS, CdS, ZnS-ReS_2, CdS-ReS_2, CdS/ZnS, and CdS/ZnS-ReS_2 under visible light irradiation for 2 h, (c) apparent quantum efficiency under irradiation with monochromatic light at different wavelengths, and (d) recycling for hydrogen evolution of CdS/ZnS-ReS_2.

the excitation of visible light. To demonstrate the change in energy band structure, we determined the conduction band position of the samples using Mott−Schottky curves (Figure 5c) and calculated the approximate valence band position using E_q. The conduction band of CdS/ZnS-ReS_2 becomes more negative, which is more favorable for the reduction reaction. In addition, we performed photoelectrochemical and photoluminescence tests on the samples to further investigate the effect of the ReS_2 cocatalyst in charge transfer. We can easily see from Figure 5d that the photocurrent response of CdS/ZnS-ReS_2 is much higher than that of CdS/ZnS, which indicates that ReS_2 is an effective carrier for promoting photogenerated carrier migration. The migration characteristics of photogenerated carriers were measured by electrochemical impedance, as shown in Figure 5e. The radius of CdS/ZnS-ReS_2 is significantly smaller than that of CdS/ZnS, indicating that the charge transfer resistance of CdS/ZnS-ReS_2 is relatively low, and the migration of photogenerated carriers is accelerated and the carrier separation is promoted, which proves that ReS_2 is an excellent cocatalyst. The lower intensity of the CdS/ZnS-ReS_2 peak in the PL spectrum indicates that ReS_2 can effectively inhibit the recombination of electron−hole pairs and accelerate carrier separation (Figure 5f).

The photocatalytic properties of the samples were investigated because of the properties of ReS_2 in promoting light absorption and photogenerated charge separation. The hydrogen production performance of the CdS/ZnS-ReS_2 samples under visible light irradiation and with NaS_2−$NaSO_3$ as the sacrificial reagent is shown in Figure 6a, with 21 445 μmol g^{-1} H_2 produced for 2 h. Figure 6b shows the photocatalytic hydrogen production rate of each of the six different samples, and we can see that the rate of hydrogen produced by the CdS/ZnS-ReS_2 sample is about 178 times higher than that of pure CdS and about 5 times higher than that of CdS/ZnS. This indicates that the photocatalytic performance can be greatly enhanced by forming CdS/ZnS heterojunctions and using ReS_2 as a cocatalyst. To better understand the details of photocatalytic hydrogen precipitation, we calculated the quantum efficiency (AQY) of CdS/ZnS-ReS_2 under different wavelengths of irradiation. The AQY of CdS/ZnS-ReS_2 was 1.3, 1.7, 1.5, and 0.026% at wavelengths of 400, 420, 500, and 550 nm, respectively (Figure 6c). The results showed that the best photocatalytic hydrogen precipitation performance was achieved at the incident wavelength of 420 nm. Since CdS is liable to photocorrosion under light, a cyclic test was conducted on the CdS/ZnS-ReS_2 sample. As shown in Figure 6d, the performance of the sample did not decrease after 8 h of illumination and still had good photocatalytic hydrogen production performance. The above results demonstrate that CdS/ZnS-ReS_2 is a promising photocatalyst with high photocatalytic activity and good cycling stability.

The possible photocatalytic mechanism of the CdS/ZnS-ReS_2 photocatalyst is shown in Figure 7. A typical heterostructure is formed between CdS and ZnS, in which ReS_2 acts as a bridge. Under the irradiation of visible light, both CdS and ZnS can be excited to produce electrons and holes. After ZnS is excited by light, electrons migrate from the valence band to the conduction band, and then the electrons in the conduction band of ZnS will be transferred to the conduction band of ReS_2, which acts as an electron transfer bridge and continues to transfer electrons to the valence band of CdS, which can well suppress the compounding of photogenerated carriers. Finally, the electrons migrate to the

https://doi.org/10.1021/acsomega.2c08110
ACS Omega 2023, 8, 6059−6066

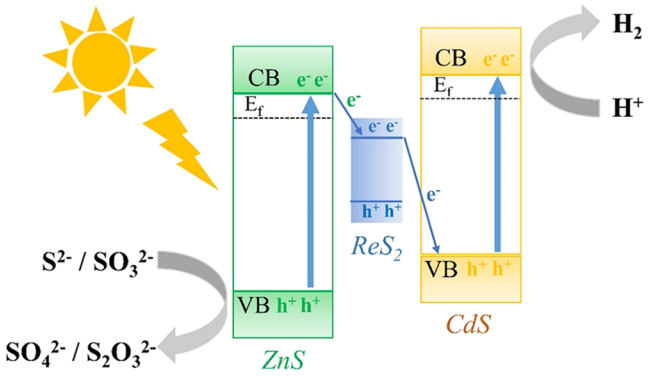

Figure 7. Schematic illustration of the proposed mechanism for the photocatalytic H_2 evolution.

conduction band of CdS and react with H^+ to form H_2. The presence of the ReS_2 intermediate can effectively inhibit the carrier complexation and promote the photogenerated charge migration, which can further enhance the photocatalytic activity of the photocatalyst.

4. CONCLUSIONS

In this study, we successfully synthesized a CdS/ZnS-ReS_2 photocatalyst by a simple hydrothermal method and used it for photocatalytic hydrogen production. CdS/ZnS-ReS_2 has favorable photocatalytic activity, with the highest hydrogen production rate of 10722 μmol g^{-1} h^{-1} under visible light irradiation, which is about 178 times higher than that of pure CdS and 5 times higher than that of CdS/ZnS. The highest AQY is 1.7% at a wavelength of 420 nm. More significantly, the photocatalytic performance did not drop after four photocycles; the heterojunction between CdS and ZnS can effectively suppress the photocorrosion defects of CdS in visible light, and the loading of ReS_2 as a cocatalyst can further promote the migration of photogenerated carriers and suppress the complexation of electron−hole pairs, so that CdS/ZnS-ReS_2 exhibits better photocatalytic performance. It is expected that this work will promote the development of photocatalytic hydrogen production technology.

AUTHOR INFORMATION

Corresponding Authors

Yang Bai − *School of New Energy and Materials, Southwest Petroleum University, Chengdu 610500, China; State Key Laboratory of Oil and Gas Reservoir Geology and Exploitation, School of Oil & Natural Gas Engineering, Southwest Petroleum University, Chengdu 610500, China*; Email: 281824767@qq.com

Liqun Ye − *College of Materials and Chemical Engineering, Key Laboratory of Inorganic Nonmetallic Crystalline and Energy Conversion Materials, China Three Gorges University, Yichang 443002, China*; orcid.org/0000-0001-6410-689X; Email: lqye@ctgu.edu.cn

Authors

Na Su − *School of New Energy and Materials, Southwest Petroleum University, Chengdu 610500, China*; orcid.org/0000-0002-5527-4135

Zhonglian Shi − *College of Materials and Chemical Engineering, Key Laboratory of Inorganic Nonmetallic Crystalline and Energy Conversion Materials, China Three Gorges University, Yichang 443002, China*

Jiale Li − *College of Materials and Chemical Engineering, Key Laboratory of Inorganic Nonmetallic Crystalline and Energy Conversion Materials, China Three Gorges University, Yichang 443002, China*

Yixue Xu − *College of Materials and Chemical Engineering, Key Laboratory of Inorganic Nonmetallic Crystalline and Energy Conversion Materials, China Three Gorges University, Yichang 443002, China*; orcid.org/0000-0001-6683-6124

Daoxiong Li − *State Key Laboratory of Oil and Gas Reservoir Geology and Exploitation, School of Oil & Natural Gas Engineering, Southwest Petroleum University, Chengdu 610500, China*

Baolu Li − *School of New Energy and Materials, Southwest Petroleum University, Chengdu 610500, China*

Yi He − *School of Chemistry and Chemical Engineering, Southwest Petroleum University, Chengdu 610500, China*; orcid.org/0000-0002-3637-8043

Complete contact information is available at: https://pubs.acs.org/10.1021/acsomega.2c08110

Notes

The authors declare no competing financial interest.

ACKNOWLEDGMENTS

This work was supported by the National Natural Science Foundation of China (nos. 52274008, 51872147, 22136003), National Key R & D Projects (no. 2019YFA0708303) and Science and Technology Cooperation Project of the CNPC-SWPU Innovation Alliance (nos. 2020CX040102, 2020CX040201).

REFERENCES

(1) Chandrasekaran, S.; Yao, L.; Deng, L.; Bowen, C.; Zhang, Y.; Chen, S.; Lin, Z.; Peng, F.; Zhang, P. Recent advances in metal sulfides: from controlled fabrication to electrocatalytic, photocatalytic and photoelectrochemical water splitting and beyond. *Chem. Soc. Rev.* **2019**, *48*, 4178−4280.

(2) Tanaka, A.; Teramura, K.; Hosokawa, S.; Kominami, H.; Tanaka, T. Visible light-induced water splitting in an aqueous suspension of a plasmonic Au/TiO_2 photocatalyst with metal cocatalysts. *Chem. Sci.* **2017**, *8*, 2574−2580.

(3) Ren, D.; Shen, R.; Jiang, Z.; Lu, X.; Li, X. Highly efficient visible-light photocatalytic H_2 evolution over 2D−2D CdS/Cu_7S_4 layered heterojunctions. *Chin. J. Catal.* **2020**, *41*, 31−40.

(4) Reece, S. Y.; Hamel, J. A.; Sung, K.; Jarvi, T. D.; Esswein, A. J.; Pijpers, J. J. H.; Nocera, D. G. Wireless Solar Water Splitting Using Silicon-Based Semiconductors and Earth-Abundant Catalysts. *Science* **2011**, *334*, 645−648.

(5) Fujishima, A.; Honda, K. Electrochemical photolysis of water at a semiconductor electrode. *Nature* **1972**, *238*, 37−38.

(6) Zhang, X.-Y.; Li, H.; Cui, X.; Lin, Y. Graphene/TiO_2 nanocomposites: synthesis, characterization and application in hydrogen evolution from water photocatalytic splitting. *J. Mater. Chem.* **2010**, *20*, 2801−2806.

(7) Wang, C.; Li, A.; Li, C.; Zhang, S.; Li, H.; Zhou, X.; Hu, L.; Feng, Y.; Wang, K.; Zhu, Z.; Shao, R.; Chen, Y.; Gao, P.; Mao, S.; Huang, J.; Zhang, Z.; Han, X. Ultrahigh Photocatalytic Rate at a Single-Metal-Atom-Oxide. *Adv. Mater.* **2019**, *31*, No. 1903491.

(8) Zhang, L.; Jin, Z.; Tsubaki, N. Zeolitic Imidazolate Framework-67-Derived P-Doped Hollow Porous Co_3O_4 as a Photocatalyst for Hydrogen Production from Water. *ACS Appl. Mater. Interfaces* **2021**, *13*, 50996−51007.

https://doi.org/10.1021/acsomega.2c08110
ACS Omega 2023, 8, 6059−6066

(9) Liu, M.; Chen, Y.; Su, J.; Shi, J.; Wang, X.; Guo, L. Photocatalytic hydrogen production using twinned nanocrystals and an unanchored NiS_x cocatalyst. *Nat. Energy* **2016**, *1*, No. 16151.
(10) Tan, C.-L.; Qi, M.; Tang, Z.; Xu, Y. Cocatalyst decorated $ZnIn_2S_4$ composites for cooperative alcohol conversion and H_2 evolution. *Appl. Catal., B* **2021**, *298*, No. 120541.
(11) Pan, R.; Hu, M.; Liu, J.; Li, D.; Wan, X.; Wang, H.; Li, Y.; Zhang, X.; Wang, X.; Jiang, J.; Zhang, J. Two-Dimensional All-in-One Sulfide Monolayers Driving Photocatalytic Overall Water Splitting. *Nano Lett.* **2021**, *21*, 6228−6236.
(12) Cheng, L.; Xiang, Q.; Liao, Y.; Zhang, H. CdS-Based photocatalysts. *Energy Environ. Sci.* **2018**, *11*, 1362−1391.
(13) Liu, Y.; Wang, B.; Zhang, Q.; Yang, S.; Li, Y.; Zuo, J.; Wang, H.; Peng, F. A novel bicomponent Co_3S_4/Co@C cocatalyst on CdS, accelerating charge separation for highly efficient photocatalytic hydrogen evolution. *Green Chem.* **2020**, *22*, 238−247.
(14) Simon, T.; Bouchonville, N.; Berr, M. J.; Vaneski, A.; Adrovic, A.; Volbers, D.; Wyrwich, R.; Doblinger, M.; Susha, A. S.; Rogach, A. L.; Jackel, F.; Stolarczyk, J. K.; Feldmann, J. Redox shuttle mechanism enhances photocatalytic H_2 generation on Ni-decorated CdS nanorods. *Nat. Mater.* **2014**, *13*, 1013−1018.
(15) Li, Q.; Guo, B.; Yu, J.; Ran, J.; Zhang, B.; Yan, H.; Gong, J. R. Highly efficient visible-light-driven photocatalytic hydrogen production of CdS-cluster-decorated graphene nanosheets. *J. Am. Chem. Soc.* **2011**, *133*, 10878−10884.
(16) Zhang, Z.-W.; Li, Q.; Qiao, X.; Hou, D.; Li, D. One-pot hydrothermal synthesis of willow branch-shaped MoS_2/CdS heterojunctions for photocatalytic H_2 production under visible light irradiation. *Chin. J. Catal.* **2019**, *40*, 371−379.
(17) Zhang, L.; Jiang, X.; Jin, Z.; Tsubaki, N. Spatially separated catalytic sites supplied with the CdS−MoS_2−In_2O_3 ternary dumbbell S-scheme heterojunction for enhanced photocatalytic hydrogen production. *J. Mater. Chem. A* **2022**, *10*, 10715−10728.
(18) Zhao, Y.; Lu, Y.; Chen, L.; Wei, X.; Zhu, J.; Zheng, Y. Redox Dual-Cocatalyst-Modified CdS Double-Heterojunction Photocatalysts for Efficient Hydrogen Production. *ACS Appl. Mater. Interfaces* **2020**, *12*, 46073−46083.
(19) Zhang, L.; Fu, X.; Meng, S.; Jiang, X.; Wang, J.; Chen, S. Ultra-low content of Pt modified CdS nanorods: one-pot synthesis and high photocatalytic activity for H_2 production under visible light. *J. Mater. Chem. A* **2015**, *3*, 23732−23742.
(20) Yin, X.-L.; Li, L.; Jiang, W.; Zhang, Y.; Zhang, X.; Wan, L.; Hu, J. MoS_2/CdS Nanosheets-on-Nanorod Heterostructure for Highly Efficient Photocatalytic H_2 Generation under Visible Light Irradiation. *ACS Appl. Mater. Interfaces* **2016**, *8*, 15258−15266.
(21) Lin, Y.; Zhang, Q.; Li, Y.; Liu, Y.; Xu, K.; Huang, J.; Zhou, X.; Peng, F. The Evolution from a Typical Type-I CdS/ZnS to Type-II and Z-Scheme Hybrid Structure for Efficient and Stable Hydrogen Production under Visible Light. *ACS Sustainable Chem. Eng.* **2020**, *8*, 4537−4546.
(22) Wang, J.; Wang, Z.; Li, L.; Chen, J.; Zheng, J.; Jia, S.; Zhu, Z. Structure-controlled CdS(0D, 1D, 2D) embedded onto 2D ZnS porous nanosheets for highly efficient photocatalytic hydrogen generation. *RSC Adv.* **2017**, *7*, 24864−24869.
(23) Zhang, J.; Wang, Y.; Zhang, J.; Lin, Z.; Huang, F.; Yu, J. Enhanced photocatalytic hydrogen production activities of Au-loaded ZnS flowers. *ACS Appl. Mater. Interfaces* **2013**, *5*, 1031−1037.
(24) Huang, L.; Wang, X.; Yang, J.; Liu, G.; Han, J.; Li, C. Dual Cocatalysts Loaded Type I CdS/ZnS Core/Shell Nanocrystals as Effective and Stable Photocatalysts for H_2 Evolution. *J. Phys. Chem. C* **2013**, *117*, 11584−11591.
(25) Niu, X.; Zhao, Y.; Wang, F.; Wu, J.; Qu, F.; Tan, W. Ultrasensitive Photoelectrochemical Biosensor Based on Novel Z-Scheme Heterojunctions of Zn-Defective CdS/ZnS for MicroRNA Assay. *Anal. Chem.* **2021**, *93*, 17134−17140.
(26) Xie, Y.; Yu, Z.; Liu, G.; Ma, X.; Cheng, H. CdS−mesoporous ZnS core−shell particles for efficient and stable photocatalytic hydrogen evolution under visible light. *Energy Environ. Sci.* **2014**, *7*, 1895−1901.
(27) Sun, G.; Shi, J.; Mao, S.; Ma, D.; He, C.; Wang, H.; Cheng, Y. Dodecylamine coordinated tri-arm CdS nanorod wrapped in intermittent ZnS shell for greatly improved photocatalytic H_2 evolution. *Chem. Eng. J.* **2022**, *429*, No. 132382.
(28) Wang, F.; Le, S.; Song, F.; Su, Y. Self-defective ZnS mediated charge transfer for bran-new inter-step mode with boosted photoactivity and enhanced photostability. *Int. J. Hydrogen Energy* **2021**, *46*, 2103−2116.
(29) Zhang, X.; Li, Y.; Zhao, J.; Wang, S.; Li, Y.; Dai, H.; Sun, X. Advanced three-component ZnO/Ag/CdS nanocomposite photoanode for photocatalytic water splitting. *J. Power Sources* **2014**, *269*, 466−472.
(30) Tada, H.; Mitsui, T.; Kiyonaga, T.; Akita, T.; Tanaka, K. All-solid-state Z-scheme in CdS-Au-TiO_2 three-component nanojunction system. *Nat. Mater.* **2006**, *5*, 782−786.
(31) Kong, L.; Dong, Y.; Jiang, P.; Wang, G.; Zhang, H.; Zhao, N. Light-assisted rapid preparation of a Ni/g-C_3N_4 magnetic composite for robust photocatalytic H_2 evolution from water. *J. Mater. Chem. A* **2016**, *4*, 9998−10007.
(32) He, B.; Bie, C.; Fei, X.; Cheng, B.; Yu, J.; Ho, W.; Al-Ghamdi, A. A.; Wageh, S. Enhancement in the photocatalytic H_2 production activity of CdS NRs by Ag_2S and NiS dual cocatalysts. *Appl. Catal., B* **2021**, *288*, No. 119994.
(33) Lu, L.; Xu, X.; An, K.; Wang, Y.; Shi, F. Coordination Polymer Derived NiS@g-C_3N_4 Composite Photocatalyst for Sulfur Vacancy and Photothermal Effect Synergistic Enhanced H_2 Production. *ACS Sustainable Chem. Eng.* **2018**, *6*, 11869−11876.
(34) Xiang, Q.; Cheng, F.; Lang, D. Hierarchical Layered WS_2/Graphene-Modified CdS Nanorods for Efficient Photocatalytic Hydrogen Evolution. *ChemSusChem* **2016**, *9*, 996−1002.
(35) Guo, L.; Yu, G.; Zhao, H.; Xing, C.; Hu, Y.; Chen, T.; Li, X. Construction of heterojunctions between ReS_2 and twin crystal $Zn_xCd_{1-x}S$ for boosting solar hydrogen evolution. *New J. Chem.* **2021**, *45*, 5137−5145.
(36) Liu, W.; Wang, P.; Ao, Y.; Chen, J.; Gao, X.; Jia, B.; Ma, T. Directing Charge Transfer in a Chemical-Bonded $BaTiO_3$@ReS_2 Schottky Heterojunction for Piezoelectric Enhanced Photocatalysis. *Adv. Mater.* **2022**, *34*, No. 2202508.
(37) Zhang, Q.; Wang, W.; Zhang, J.; Zhu, X.; Fu, L. Thermally Induced Bending of ReS_2 Nanowalls. *Adv. Mater.* **2018**, *30*, No. 1704585.
(38) Xing, C.; Zhao, H.; Yu, G.; Guo, L.; Hu, Y.; Chen, T.; Jiang, L.; Li, X. Modification of g-C_3N_4 Photocatalyst with Flower-like ReS_2 for Highly Efficient Photocatalytic Hydrogen Evolution. *ChemCatChem* **2020**, *12*, 6385−6392.
(39) Ran, J.; Zhang, H.; Qu, J.; Shan, J.; Chen, S.; Yang, F.; Zheng, R.; Cairney, J.; Song, L.; Jing, L.; Qiao, S. Atomic-Level Insights into the Edge Active ReS_2 Ultrathin Nanosheets for High-Efficiency Light-to-Hydrogen Conversion. *ACS Mater. Lett.* **2020**, *2*, 1484−1494.
(40) Ye, L.; Ma, Z.; Deng, Y.; Ye, Y.; Li, W.; Kou, M.; Xie, H.; Zhikun, X.; Zhou, Y.; Xia, D.; Wong, P. K. Robust and efficient photocatalytic hydrogen generation of ReS_2/CdS and mechanistic study by on-line mass spectrometry and in situ infrared spectroscopy. *Appl. Catal., B* **2019**, *257*, No. 117897.
(41) Zhao, H.; Fu, H.; Yang, X.; Xiong, S.; Han, D.; An, X. MoS_2/CdS rod-like nanocomposites as high-performance visible light photocatalyst for water splitting photocatalytic hydrogen production. *Int. J. Hydrogen Energy* **2022**, *47*, 8247−8260.

https://doi.org/10.1021/acsomega.2c08110
ACS Omega 2023, 8, 6059−6066